JOURNAL OF SOLID STATE CHEMISTRY 83, 282–291 (1989)

Defect Solid State Chemistry of Magnetoplumbite Structured Ceramic Oxides.

I. $SrAl_{12}O_{19}$

L. XIE AND A. N. CORMACK

New York State College of Ceramics, Alfred University, Alfred, New York 14802

Received April 17, 1989; in revised form August 4, 1989

Computer atomistic simulation techniques have been used to investigate defect solid state chemistry in $SrAl_{12}O_{19}$. Our calculations show that transferring interatomic potential parameters from models of binary oxides provides adequate models of the magnetoplumbite structure. Schottky disorder is found to be the dominant defect mode in $SrAl_{12}O_{19}$. When Sr and Al in $SrAl_{12}O_{19}$ are replaced by La and Mg, Mg prefers to occupy 4*f* Al(3) tetrahedral sites. © 1989 Academic Press, Inc.

1. Introduction

Ceramic oxides with the magnetoplumbite crystal structure have been receiving considerable attention recently, because of their diverse applications. Those based on Fe_2O_3 are of interest for microwave applications and for data storage in magnetic bubble devices (*1, 2*). They are used in thin layer forms, and such layers must be grown epitaxially on nonmagnetic isotypic single crystal substrates such as magnetoplumbite crystals based on Al_2O_3, having matching or similar lattice constants.

Our present concern is those based on Al_2O_3. The main interest in the magnetoplumbite-type lanthanide aluminates with the formula $Ln^{3+}M^{2+}Al_{11}O_{19}$ (Ln^{3+} = La^{3+}, Ce^{3+}, Pr^{3+}, Eu^{3+}, and Nd^{3+}; M^{2+} = Mg^{2+}, Mn^{2+}, Ni^{2+}, and Co^{2+}) lies in their potential use as laser (*3, 4*) and luminescent materials (*5, 6*). They also have been proposed as hosts for radioactive waste disposal (*7, 8*) and in the single crystal form, they may be good substrates for LPE (liquid phase epitaxy) growth of rare earth hexaferrite thin films (*9, 10*).

The actual use of these materials will be dictated, of course, by the details of their solid state chemistry, in particular their defect chemistry. The composition for an ideal magnetoplumbite phase based on Al_2O_3 is $MAl_{12}O_{19}$ (where M is typically an alkaline earth such as Sr or Ca) which has a hexagonal structure, with space group $P6_3/mmc$. The unit cell (Fig. 1) is built of spinel-like blocks containing Al^{3+} cations separated by mirror planes which contain one Sr^{2+} and three oxygen atoms per unit cell (*11*); the Wyckoff position of cations and their coordination polyhedra are gathered together in Table I.

It has been found that alumina based magnetoplumbites exhibit a wide range of chemistry and nonstoichiometry whose origin obviously lies in the defect structure of the material. The divalent cation can be replaced completely by a trivalent ion such as La^{3+} or other rare earth species (hence the lasing interests: the cation sites in the mir-

0022-4596/89 $3.00

ror plane are well separated) with compensation by a different cation such as Mg^{2+} substitution for Al^{3+} in the spinel slabs. Because of the complexity of the basic crystal structure, however, little progress has been made experimentally toward identifying the intrinsic defect structure. For example, the distribution of Mg over the possible Al sites has not been determined conclusively; in fact, several different schemes have been proposed of which there are two principle conflicting variations (*12, 13*). This is a major drawback to optimal development of these materials.

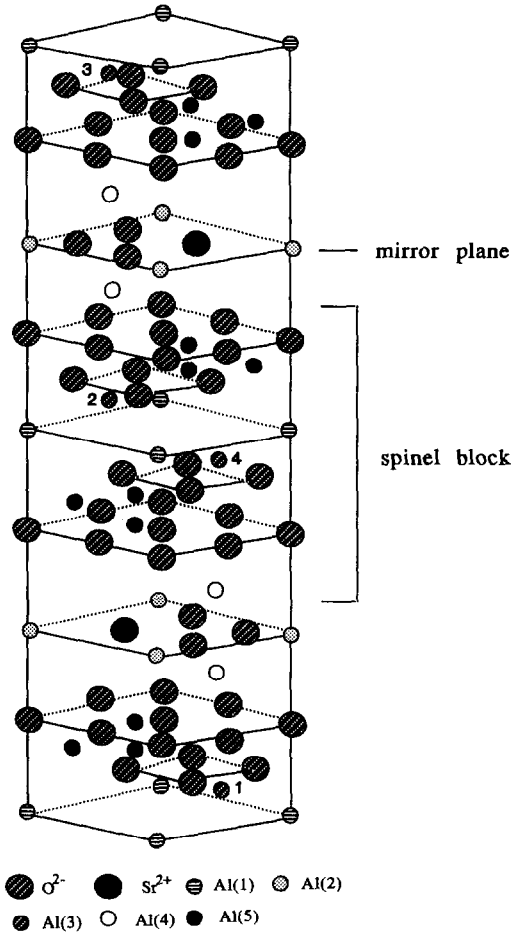

FIG. 1. The magnetoplumbite unit cell of $SrAl_{12}O_{19}$.

TABLE I

SOME CHARACTERISTICS OF THE DIFFERENT CATION SITES AVAILABLE FOR Al^{3+} OR Mg^{2+} IN THE M.P. STRUCTURE

	Wyckoff position	Site symmetry	Coordination
Regular octahedron	Al(1) 2*a*	D_{3d}	6
Trigonal bipyramid	Al(2) 2*b*	C_{3v}	5
Tetrahedron	Al(3) 4*f*	C_{3v}	4
Distorted octahedron	Al(4) 12*k*	C_s	6
Antiprism	Al(5) 4*f*	C_{3v}	6

We have used computer simulation methods to discover the intrinsic defect structure and hence determine how the defects will affect the solid state chemistry of alumina based magnetoplumbites. In this paper we report the establishment of a suitable interatomic potential model for Sr $Al_{12}O_{19}$ and show how this is used to obtain information about the occupancy preference of Mg^{2+} over the possible sites in the spinel blocks when Sr^{2+} and Al^{3+} are replaced by La^{3+} and Mg^{2+}.

2. Simulation Techniques

2.1. Potential Models

A potential model must describe the interaction of each pair of ions, so that the lattice energy between them can be determined; i.e.,

$$U = \frac{1}{2}\sum_i \sum_j (q_i q_j / r_{ij} + V_{ij}), \qquad (1)$$

where r_{ij} is the distance between the ions. The first term of the cohesive energy is the long-range coulombic interaction corresponding to the interaction between charge. For the present study, we used full ionic charges, i.e., Al^{3+}, Sr^{2+}, and O^{2-}. The second part of the lattice energy consists of two terms: a short-range, parameterized, two-body interaction term and an electronic polarizability term.

The two-body, short-range, noncoulombic interactions were described by a simple analytical Buckingham function,

$$V(_{ij}) = A_{ij} \exp(-r_{ij}/\rho_{ij}) - C_{ij} r_{ij}^{-6}. \quad (2)$$

The short-range interaction includes both the repulsive forces due to the overlap of ion charge clouds, and an attractive term due to dispersive interactions. The simulation of polarizability in the ions that constitute the lattice is included through the shell models originally developed by Dick and Overhauser (*14*). This model consists of a simple mechanical representation of the ionic dipole. The polarizable valence shell electrons are represented by a massless shell which is connected to the core by a harmonic spring. Potential parameters (A, ρ, and C), with the appropriate shell charges, Y, and spring constant, k, were taken from the compilation of Lewis and Catlow (*15*) and are listed in Table II. We did not find it necessary to modify the short-range parameters and only minor adjustments to the shell model parameters were needed. This experience suggests that interactions may be transferred from compound to compound under the appropriate circumstances. The short-range potential cutoff, the interatomic separation beyond which the potential is assumed to be negligible, is 1.89 lattice units (10.51 Å).

TABLE II
INTERIONIC POTENTIALS

(A) Short-range parameters for potential form $V(r) = Ae^{-r/\rho} - Cr^{-6}$

Interaction	A (eV)	ρ (Å)	C (eV Å^{-6})
Mg–O	1644.980	0.36196	0.000
Sr–O	1400.000	0.3500	0.000
La–O	1428.500	0.29453	0.000
Al–O	1474.400	0.30059	0.000
O–O	22764.200	0.14910	17.890

(B) Shell parameters

Interaction	Shell charge (Y/e)	Spring constant k (eV Å^{-2})
Sr(core)–Sr(shell)	1.330	21.53
La(core)–La(shell)	3.000	99,999.99
Mg(core)–Mg(shell)	2.000	99,999.99
Al(core)–Al(shell)	3.000	99,999.99
O(core)–O(shell)	−2.207	27.290

2.2. *Perfect Lattice Simulations*

The cohesive energy, from the Born model (for a static lattice), is

$$U = \frac{1}{2} \sum_i \sum_j (q_i q_j / r_{ij} + A_{ij} \exp((-r_{ij}/\rho_{ij}) - C_{ij} r_{ij}^{-6}), \quad (3)$$

where the summations refer to all pairs of ions i and j in the crystal. The lattice energy is thus calculated exactly and the only limitations in the procedure are due to deficiencies in the interatomic potentials. Calculations of the crystal energy of the structure under investigation are combined with efficient minimization procedures to determine the equilibrium configuration, which may then be compared with experimental structure. A Newton-like second derivative method is used in the energy minimization. In our approach, all the atomic coordinates within the unit cell (not just the symmetry independent ones) are allowed to relax to find the minimum energy configuration. During the atomic coordination relaxation, the lattice vectors are kept fixed. After a minimum energy configuration has been found, the lattice vectors may be relaxed using elasticity theory and the calculated residual bulk lattice strains, as described by Cormack (*16*). This procedure is repeated iteratively until all remaining strains (both on the unit cell vectors and atomic coordinates) have been removed. It is possible to let all the structural variables, basis vectors, and unit cell vectors relax at the same time, but this can lead to some messy numerical problems that are avoided using the iterative approach. This approach does not

require space group symmetry to be conserved, although we would expect, if the initial configuration is close to equilibrium, such symmetry to be retained. This may be tested by deliberately distorting the initial structure to remove the symmetry.

Comparison between the calculated structure and its X-ray counterpart constitutes a test of the viability of the interatomic potential model. The acceptable agreement we report here indicates that the model is, indeed, adequate.

2.3. *Defect Energy Calculations*

Calculations of defect structures and energies introduce one vital feature additional to those for the perfect lattice methods. This is the occurrence of relaxation of lattice atoms around the defect species. The effect is large because the defect generally provides an extensive perturbation of the surrounding lattice, and, in the case of ionic crystals, the relaxation field is long range as the perturbation provided by the defect is mainly coulombic in origin.

The simulation techniques used in this study were based on a generalized Mott–Littleton (*17*) approach, where the important feature is that the crystal surrounding the defect is divided into two regions. The outer region II is treated as a polarizable dielectric continuum, while the coordinates of the distorted inner region I are explicitly relaxed using appropriate interatomic potentials.

Following the division of the crystal into the two regions, the following formal equation for the total defect formation energy may be written,

$$E = E_1(x) + E_2(x, y) + E_3(y), \qquad (4)$$

where E_1 is a function of the coordinates x (and dipole moments) of the ions solely within the region I, E_3 depends solely on the displacements y of the ions within II, and $E_2(x, y)$ arises from interaction between the two regions. The CASCADE code (*18*) was used in this study.

3. Results and Discussion

3.1. *Structure Refinement Using Energy Minimization Techniques*

The program METAPOCS (*19*) was used to determine the equilibrium positions for atoms in the structure as described in Section 2.2. In the present study, for $SrAl_{12}O_{19}$, the structure reported by Lindop *et al.* (*20*) was used both for comparison and as an initial setup for the calculations. With the X-ray data as the starting point, the energy of the unit cell was minimized with respect to the coordinates of all the ions. The residual bulk lattice strains were sufficiently small that we did not think it necessary to remove them. Thus the lattice vectors a = 5.562 Å and c = 21.972 Å from Ref. (*20*) were used for all the calculations. The coordinates of the equilibrated structure and the X-ray structure are reported in Table III. From this table we can see that the experimental coordinates and those obtained for the equilibrated structure are in good agreement. The success of these calculations in reproducing correctly the complex magnetoplumbite crystal structure provides evidence for the viability of the potential models used in this study, and allows us to continue with the calculation of point defect energies, which are discussed in the next section.

As was pointed out to us by one of the reviewers, one interesting crystallographic feature of the magnetoplumbite structure is the unusually large amplitude of vibration of the Al(2) cation, along the c axis, which has been interpreted as an indication of incipient tetrahedral coordination. However, it is difficult to distinguish between true thermal motion and static disorder using diffraction data. The potential well around this site can be studied computationally.

TABLE III

A COMPARISON OF THE FINAL EQUILIBRATED ATOM POSITIONS WITH THE X-RAY STRUCTURE FOR $SrO \cdot 6Al_2O_3$

Atom		Data from X-ray structure	Data from calculation	Δ^a
Sr	x	0.6667	0.6667	0.0000
	z	0.2500	0.2500	0.0000
Al(1)	x	0.0000	0.0000	0.0000
	z	0.0000	0.0000	0.0000
Al(2)	x	0.0000	0.0000	0.0000
	z	0.2500	0.2500	0.0000
Al(3)	x	0.3333	0.3333	0.0000
	z	0.0276	0.0309	0.0033
Al(4)	x	0.1685	0.1675	0.0010
	z	−0.1082	−0.1085	0.0003
Al(5)	x	0.3333	0.3333	0.0000
	z	0.1903	0.1891	0.0012
O(1)	x	0.0000	0.0000	0.0000
	z	0.1481	0.1493	0.0012
O(2)	x	0.3333	0.3333	0.0000
	z	−0.0538	−0.0541	0.0003
O(3)	x	0.1822	0.1838	0.0016
	z	0.2500	0.2500	0.0000
O(4)	x	0.1552	0.1516	0.0036
	z	0.0523	0.0527	0.0004
O(5)	x	0.5025	0.4996	0.0029
	z	0.1476	0.1446	0.0027

[a] Difference between equilibrated and X-ray structures.

With the defect simulation program CASCADE, an Al(2) cation can be systematically displaced from its crystallographic position and the potential profile along the c axis calculated. This will indicate whether or not a local minimum, with tetrahedral coordination, exists.

Our calculations show that the energy of the cation keeps increasing as it is moved along the c axis away from the Al(2) site. There is no indication of a local minimum in a tetrahedral environment. Thus we conclude that the large thermal amplitude contains no contribution from static disorder and that there is no tendency toward tetrahedral coordination for this cation. Thus the large thermal amplitudes would seem to be real, and we suggest that this is due to the large bond lengths between the Al(2) cation and the O(3) anion.

3.2. *Intrinsic Disorder*

Computer simulations are an ideal way to approach intrinsic disorder in these complex systems because each defect can be treated separately and systematically. In $SrAl_{12}O_{19}$, vacancy and interstitial formation energies are calculated for each of the possible species. From these quantities, the energies per defect for the various possible modes of disorder may be obtained. For $SrAl_{12}O_{19}$, a number of types of disorder need to be investigated. Schottky disorder, for example, involves a large number of defects, since one formula unit must be removed from the bulk. Thus we are dealing with a Schottky defect containing 32 vacancies! For nonstoichiometry, one needs to consider as well both SrO and Al_2O_3 Schottky defects. For Frenkel disorder one needs to consider interstitials of each of the three different chemical species in the unit cell in addition to their corresponding vacancies. Once the energies of the defects have been calculated, then the optimal modes of disorder may be found. Our results are gathered together in Table IV. An important point to note is that the defect energies were calculated within our equilibrated crystal structure, as given in Table III.

From the calculated energies for cation and anion vacancies and interstitials, we obtain Schottky and Frenkel defect formation energies which are also given in Table IV, as energies per constituent defect. Note that because the different types of disorder involve varying numbers of defects, comparison in terms of energy per defect is essential. The thermodynamic grounds for this have been discussed by Catlow and James (*21*). Our results show clearly that Schottky disorder is the dominant defect mode to be expected in $Sr_2Al_{12}O_{19}$.

TABLE IV

CALCULATED DEFECT ENERGIES FOR THE BASIC ATOMISTIC DEFECTS

Defect	Defect energy (eV)
Sr^{2+} vacancy	15.40
Sr^{2+} interstitial	−7.76
Al^{3+} vacancy	52.30
Al^{3+} interstitial	−45.41
O^{2-} vacancy	20.93
O^{2-} interstitial	−16.10
Al^{3+} Frenkel[a]	3.45
O^{2-} Frenkel[a]	2.42
Sr^{2+} Frenkel[a]	3.82
Schottky[a]	1.75

[a] Energy per constituent defect.

3.3. *Sr Migration Energies*

Obviously in magnetoplumbite structured compounds it is very difficult to evaluate the energetics of possible migration mechanisms from experiment. Only a macroscopic energy can usually be measured. However, our atomistic simulations can give us a theoretical guide to diffusion paths, since an activation energy can be calculated for each possible, or conjectured, mechanism. The activation energy is obtained by calculating the potential energy profile along the assumed migration path. For example, in the case of Sr vacancy migration, the "ground state" is a Sr vacancy. The vacancy migrates by changing places with a neighboring Sr ion. Actually it is the neighboring Sr ion that moves and by calculating the energy of this ion at a number of positions along the migration path, one finds the potential profile, and hence the saddlepoint energy. Thus, although ionic migration is a dynamic process, static defect energy calculations may be reasonably employed. In fast ion conductors, where the migration energy may be very low ($\approx$ 0.1–0.3 eV), it may be advisable to resort to a molecular dynamics approach. This was not considered necessary here.

Neighboring Sr sites are separated by a rather formidable obstacle, consisting of three oxygens and one aluminum lying in the mirror plane, with additional Al ions sitting above and below the oxygens. There seem to be no obviously low energy route through this obstacle, so a number of different paths were examined. All had high energies; the lowest is reported in Table V.

Clearly, if one or other of the ion positions in the "obstacle" were missing, it would be easier for the Sr ion to pass through. This prompted the calculations of vacancy assisted Sr migration.

In Fig. 2a we illustrate schematically a saddle point configuration for a simple Sr vacancy jump, and in Figs. 2b and 2c we show Sr diffusion paths in the presence of an oxygen vacancy or an Al vacancy. Vacancy assisted cation diffusion has been suggested for other systems (*22*) and given the rather close packed nature of this structure, it seemed reasonable to investigate it here. Such mechanisms are quite compatible with the idea of Schottky intrinsic disorder. The activation energies corresponding to Fig. 2 are given in Table V. It is very clear that the presence of both oxygen and aluminum vacancies decreases the activation energy of Sr migration. In the presence of Al vacancies, Sr migrates along a different diffusion path, compared with the path described in Fig. 2a or 2b. Obviously, there may be other feasible migration mechanisms which we have not considered.

TABLE V

CALCULATED ACTIVATION ENERGIES FOR Sr VACANCY MIGRATION IN $SrAl_{12}O_{19}$[a]

Saddle point configuration	Activation energy (eV)
Migration in perfect structure	20.41
Migration with $Al_{vac.}$	6.63
Migration with $O_{vac.}$	11.74

[a] Corresponding to the migration configurations in Fig. 2.

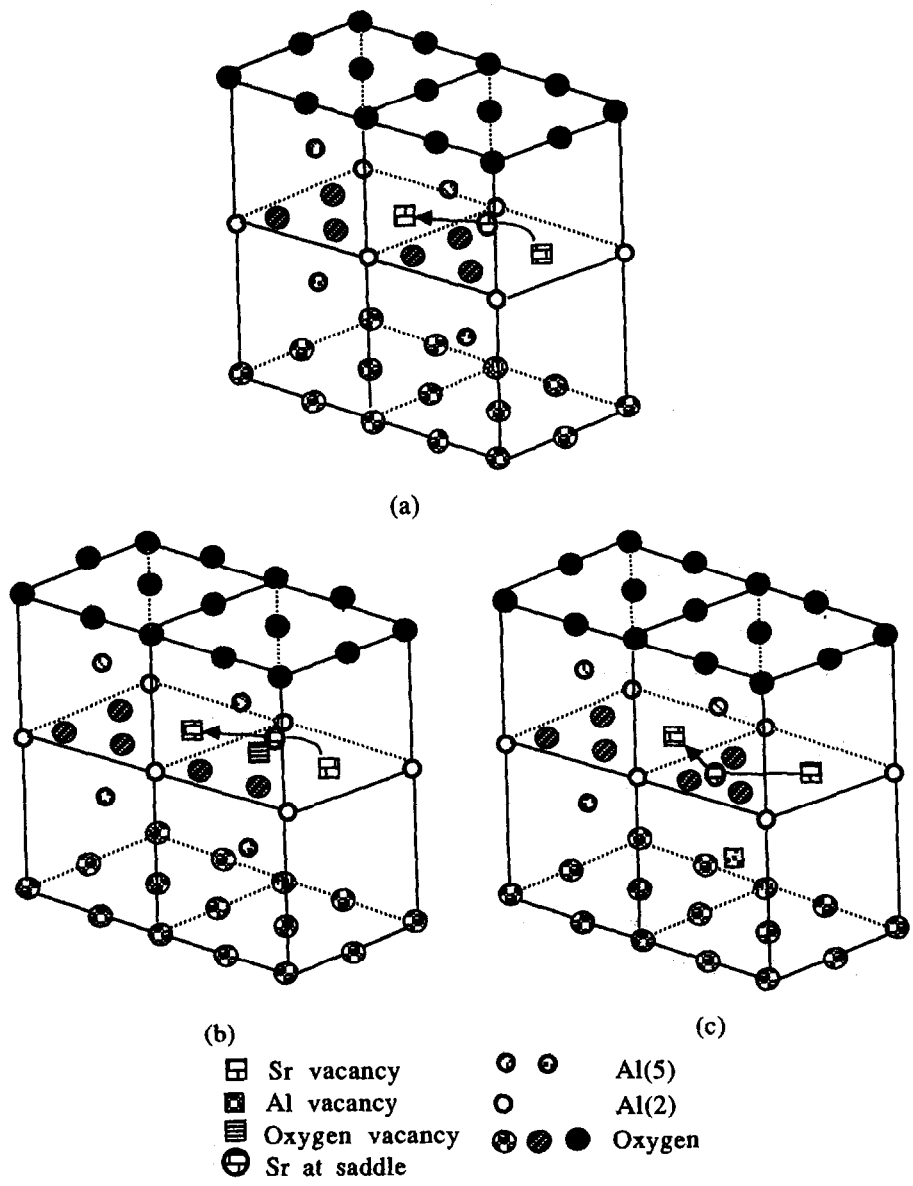

FIG. 2. Saddle point configuration for Sr vacancy migration in the magnetoplumbite structure. (a) Ideal structure, (b) with oxygen vacancy, (c) with Al vacancy.

These are very likely to involve more complex vacancy aggregates incorporating a number of Al and oxygen vacancies in their structures.

The lowest Sr vacancy activation energy which we obtain from our calculations for $SrAl_{12}O_{19}$ is 6.63 eV. The energy is still very high, compared, for example, with β''-alumina ($Na_2O \cdot MgO \cdot 5Al_2O_3$). The sodium activation energy which is obtained from the calculations of Walker and Catlow for β''-alumina is only 0.17 eV (*23*). Although

Na–β''-alumina is generally assumed to conduct via a vacancy mechanism, there is a considerable difference between the two structures of β''-alumina and magnetoplumbite which lies predominantly in the structure of the mirror planes, resulting in substantially different migration energies between Na^+ in β''-alumina and Sr^{2+} in $SrAl_{12}O_{19}$. The mirror planes of both β''-alumina and magnetoplumbite structures are shown in Fig. 3. In the conduction plane of β''-alumina, there are one Na^+ and one oxygen ion. In $SrAl_{12}O_{19}$, on the other hand, ions in the mirror plane are quite strongly trapped and therefore do not easily move. The reason for this is that the mirror plane consists of three oxygen and one Sr^{2+} and there is just no simple migration path available. This result confirms the reasoning behind the selection of the magnetoplumbite phase as a basis of mineralogical assemblages for hosting radioactive elements of nuclear waste such as ^{90}Sr, ^{137}Cs, etc. (*7*).

3.4. Cation Substitution in $SrAl_{12}O_{19}$

The magnetoplumbites, nominally $X(Al, Fe)_{12}O_{19}$, where X = Sr, Ba, $Cs_{0.5} + La_{0.5}$, $Na_{0.5} + RE_{0.5}$, have structures which may be expected to accommodate a diverse chemistry because of the variety of crystallographic sites within the unit cell. They are composed of spinel blocks, which have the usual IV and VI coordinated sites for cations, whereas the interspinel layers have rather unusual V-fold sites for small cations. The interspinel layers also provide XII-fold sites to accommodate large cations of $\simeq$1.15 to 1.84 Å radius. The large ions may be monovalent, divalent, or trivalent with balancing charge substituents either in the interspinel layer (i.e., $Na_{0.5} + La_{0.5}$) or in both the interspinel layer and the spinel block (e.g., by La^{3+} and Mg^{2+}, simultaneously replacing Sr^{2+} and Al^{3+} in $SrAl_{12}O_{19}$ to produce $LaMgAl_{11}O_{19}$). The latter reaction can be expressed as

$$SrAl_{12}O_{19} + \tfrac{1}{2}La_2O_3 + MgO \rightleftharpoons La_{Sr}Mg_{Al}Al_{11}O_{19} + SrO + \tfrac{1}{2}Al_2O_3. \quad (5)$$

The defect reaction energy for this process is

$$E = E_{La/Sr} + E_{Mg/Al} + E^{Lat.}_{SrO} + 0.5 * E^{Lat.}_{Al_2O_3} - E^{Lat.}_{MgO} - 0.5 * E^{Lat.}_{La_2O_3} = -8.08 \text{ eV}. \quad (6)$$

Some lattice energies and defect energies related to this question are given in Tables

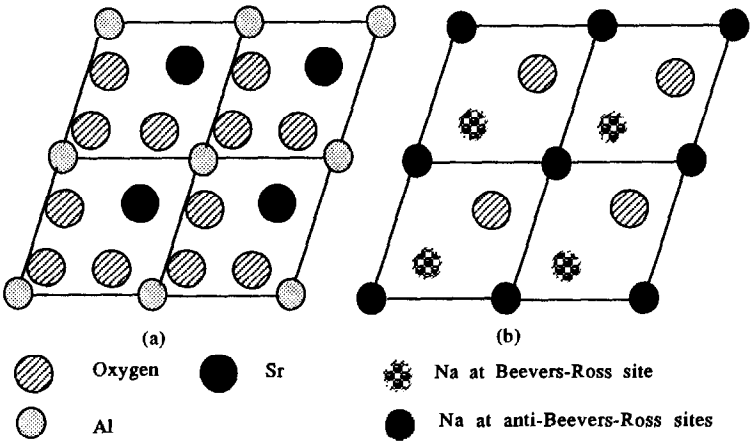

FIG. 3. (a) The mirror plane of magnetoplumbite and (b) the conduction plane of β''-alumina.

TABLE VI

THE LATTICE ENERGIES OF RELEVANT COMPOUNDS PER FORMULA UNIT

Compound	Lattice energy (eV)
$SrAl_{12}O_{19}$	−984.75
$LaMgAl_{11}O_{19}$	−975.49
SrO	−33.83
Al_2O_3	−160.31
La_2O_3	−124.00
MgO	−41.18

VI and VII. There is no question of the location of La^{3+} because of its large ion radius. La^{3+} can only substitute for Sr which is in the mirror plane 2(*d*) position. However, the question of in which particular Al^{3+} sites one may find Mg^{2+} located is not so straightforward. It is not easy to identify Mg^{2+} and Al^{3+} by X-ray diffraction, for Mg^{2+} is indistinguishable from Al^{3+} in terms of scattering factor, and until now no clear evidence has been found of its location on a particular Al site. From a structural determination of $LaMgAl_{11}O_{19}$, Lefebvre *et al.* (*12*) suggested that Mg prefers to occupy tetrahedral 4*f* and octahedral 2*a* sites; on the other hand, Abrahams *et al.* (*13*) inferred that the Mg atoms are located at Al(3) 4*f* positions, sharing a tetrahedral site equally with Al.

We have calculated the energies of Mg_{Al} substitution at different Al^{3+} sites, and the results for these energies both in the presence or absence of La_{Sr} are given in Table VII. They show clearly that Mg^{2+} ions prefer to occupy Al(3) 4*f* positions which are located within spinel block with [4] coordination when La^{3+} ions are absent or present. Our simulation results are consistent with the experimental results of Abrahams *et al.* (*13*), but not with those of Lefebvre *et al.* (*12*). The ability to distinguish between these two suggested cation distributions is a feature of atomistic simulations that we believe should be more widely exploited, especially in systems with a complex crystal chemistry.

4. Conclusions

We have shown that it is possible to model complicated crystal structures such

TABLE VII

CALCULATED DEFECT ENERGIES FOR SUBSTITUTION

Defect	Position of Mg	Defect energy (eV)
$1La_{Sr}^{2+a}$	—	−22.41
$1Mg_{Al}^{3+}$	Al(3) 4*f*	25.14
$1Mg_{Al}^{3+}$	Al(5) 4*f*	27.32
$2Mg_{Al}^{3+}$	Al(3) 4*f*	54.28
$2Mg_{Al}^{3+}$	Al(5) 4*f*	59.90
$1Mg_{Al}^{3+}$ and La_{Sr}^{2+a}	Al(3) 4*f*	4.98
$1Mg_{Al}^{3+}$ and La_{Sr}^{2+a}	Al(5) 4*f*	8.33
$1Mg_{Al}^{3+}$ and $2La_{Sr}^{2+a}$	Al(3) 4*f*	13.71
$1Mg_{Al}^{3+}$ and $2La_{Sr}^{2+a}$	Al(5) 4*f*	11.06
$2Mg_{Al}^{3+}$ and $2La_{Sr}^{2+a}$	Al(3) 4*f*	14.45
$2Mg_{Al}^{3+}$ and $2La_{Sr}^{2+a}$	Al(3) 4*f* and Al(1) 2*a*	15.83
$2Mg_{Al}^{3+}$ and $2La_{Sr}^{2+a}$	Al(3) 4*f* and Al(5) 4*f*	17.18
$2Mg_{Al}^{3+}$ and $2La_{Sr}^{2+a}$	Al(2) 2*b*	17.92
$2Mg_{Al}^{3+}$ and $2La_{Sr}^{2+a}$	Al(4) 12*k*	16.79

[a] La at 2*d* positions.

as $SrAl_{12}O_{19}$ magnetoplumbite using atomistic simulation methods coupled with energy minimization techniques. Our results indicate intrinsic disorder to be of Schottky type in the stoichiometric structure. Because the mirror plane is closepacked, the Sr^{2+} has a very high migration energy even for a vacancy mechanism in the mirror plane. In the presence of Schottky defect species such as Al or oxygen vacancies, the activation energy is decreased. Furthermore, the type of vacancies affects the diffusion path of Sr. There may well be other, more complicated, vacancy assisted migration mechanisms than we have been able to consider here.

Like other $LaMAl_{11}O_{19}$ compounds (M = Co, Mn, Fe) in which the divalent cations lie exclusively in the tetrahedral sites of the spinel blocks (*24, 25*) (as in the corresponding MAl_2O_4 spinels), in $LaMgAl_{11}O_{19}$, the Mg^{2+} ions also prefer to occupy 4*f* Al(3) tetrahedral sites as they do in $MgAl_2O_4$.

Acknowledgments

We thank the New York State College of Ceramics for financial support. Most of the calculations reported in this work were performed at the Cornell National Supercomputer Facility which is supported in part by New York State, NSF, and IBM corporation. We are grateful to one of the reviewers for pointing out the thermal behavior of the Al(2) cation.

References

1. L. G. Van Uitert, D. H. Smith, W. A. Bonner, W. H. Grokiewicz, and G. J. Zydzik, *Mater. Res. Bull.* **5,** 455 (1970).
2. H. L. Glass and F. S. Stearns, *IEEE Tran. Magn.* **13,** 1241 (1977).
3. A. Kahn, A. M. Lejus, M. Macdsac, J. Thery, and D. Vivien, *J. Appl. Phys.* **52**(11), 6864 (1981).
4. A. Kahn, A. M. Lejus, J. Thery, and D. Vivien, European Patent No. 8140, p 1087-2 (1981).
5. A. L. N. Stevels, *J. Electrochem. Soc.* **125,** 588 (1978).
6. J. M. P. J. Verstgen, J. G. Verlijsdonsk, E. P. J. de Meester, W. H. M. van de Spijker, and J. G. Verrite, US Patent No. 4216408 (1980).
7. P. E. D. Morgan, D. R. Clarke, C. M. Jantzen, and A. B. Harker, *J. Amer. Ceram. Soc.* **64**(5), 249 (1981).
8. P. E. D. Morgan and E. H. Cirlin, *J. Amer. Ceram. Soc.* **69**(11), C-114 (1982).
9. D. Lefebvre, A. Kahn, and J. Thery, *Mat. Res. Bull.* **22,** 1039 (1987).
10. J. M. Coutellier, B. Ferrand, J. Daval, Y. Grange, and J. C. Joubert, *Mat. Res. Bull.* **19,** 1037 (1984).
11. M. Gasperin and M. C. Caine, *J. Solid State Chem.* **54,** 61 (1984).
12. D. Lefebvre, J. Thery, and D. Vivien, *J. Amer. Ceram. Soc.* **69**(11), C-289 (1986).
13. S. C. Abrahams, P. Marsh, and C. D. Brandle, *J. Chem. Phys.* **86,** 4221 (1987).
14. B. G. Dick and A. W. Overhauser, *Phys. Rev.* **112,** 90 (1958).
15. G. V. Lewis and C. R. A. Catlow, *J. Phys. C* **18,** 1149 (1985).
16. A. N. Cormack, *in* "Computer Simulation of Solids" (R. A. Catlow and W. C. Mackroadt, Eds.), Chap. 20, Springer-Verlag, Berlin (1982).
17. N. F. Mott and M. J. Littleton, *Trans. Faraday Soc.* **34,** 485 (1938).
18. M. J. Norgett, Report No. AERE-R7650, A.E.R.E. Harwell, UK (1974).
19. C. R. A. Catlow, A. N. Cormack, and F. Theobald, *Acta Crystallogr. Ser. B* **40,** 195 (1984).
20. A. J. Lindop, C. Matthews, and D. W. Goodwin, *Acta Crystallogr. Ser. B* **31,** 2940 (1975).
21. C. R. A. Catlow and R. James, *Proc. R. Soc. (London) Ser. A* **384,** 157 (1982).
22. P. W. E. Jacobs and D. A. MacDonaill, *Solid State Ionics* **23,** 295 (1987).
23. J. R. Walker and C. R. A. Catlow, *J. Phys. C* **15,** 6151 (1982).
24. F. Laville, M. Perrin, A. M. Lejus, M. Gasperin, R. Moncorge, and D. Vivien, *J. Solid State Chem.* **65,** 301 (1986).
25. Like Xie and A. N. Cormack, to be published.